corrosion and materials degradation

MDPI

Article

Cathodic Protection of Complex Carbon Steel Structures in Seawater

Philippe Refait [1,*], Anne-Marie Grolleau [2], Marc Jeannin [1] and René Sabot [1]

[1] LaSIE, UMR 7356 CNRS, La Rochelle Université, 17000 La Rochelle, France
[2] CESMAN/CM Naval Group Research, Marine Corrosion & Cathodic Protection Department, 50104 Cherbourg-en-Cotentin, France
* Correspondence: prefait@univ-lr.fr; Tel.: +33-5-46-45-82-27

Abstract: Cathodic protection efficiency of complex carbon steel structures in confined seawater environment was studied using a specific experimental device. Schematically, this device consisted of a Plexiglas matrix, crossed by a channel 50 cm long, 5 mm deep, 1.5 to 5 cm wide, which moreover included four bends at 90°. Seawater flowed continuously inside the channel over 12 steel coupons embedded in the Plexiglas matrix. Cathodic protection was applied at a constant potential of −1060 mV vs. Ag/AgCl-seawater with respect to a reference electrode located outside the channel, at the seawater flow entry. The potential of four selected coupons was monitored over time via a microelectrode set close to each coupon. It varied significantly with the distance separating the coupons from the channel entry. At the end of the 3.5-month experiment, a polarization curve was acquired. The residual corrosion rate under cathodic protection was estimated via the extrapolation of the anodic Tafel line. It varied from <1 μm yr^{-1} to 16 μm yr^{-1}, depending on the potential reached by the coupon (between −900 and −1040 mV vs. Ag/AgCl-seawater) at the end of the experiment and on the properties of the calcareous deposit formed on the steel surface.

Keywords: seawater; cathodic protection; carbon steel; calcareous deposit; marine renewable energy

Citation: Refait, P.; Grolleau, A.-M.; Jeannin, M.; Sabot, R. Cathodic Protection of Complex Carbon Steel Structures in Seawater. *Corros. Mater. Degrad.* **2022**, *3*, 439–453. https://doi.org/10.3390/cmd3030026

Academic Editor: María Criado Sanz

Received: 11 July 2022
Accepted: 9 August 2022
Published: 12 August 2022

1. Introduction

Marine Renewable Energy (MRE) devices such as offshore wind turbines or ocean current turbines involve carbon steel structures with complex geometries and/or inner channels of small dimension where seawater may flow. In most cases, cathodic protection (CP) is envisioned to ensure the durability of the immersed part of the MRE devices. Modelling, predicting and quantifying the efficiency of CP for such complex structures may be challenging. Consequently, specific experimental data may be necessary for a reliable modelling of the CP system. An experimental device was designed to simulate a complex steel structure where seawater would flow inside a channel of small dimension. The steel structure inside the channel was mimicked by a series of 12 steel coupons connected to each other. Four of them could be disconnected individually from the system to be studied separately. In the channel, due to the small cross-sectional area, an important ohmic drop should increase the potential of the metal so that deep inside the channel an insufficient cathodic potential could prevail.

In seawater, the increase of the interfacial pH due to CP induces the formation of a mineral layer on the steel surface. At the potentials usually used for CP of carbon steel, this layer is mainly composed of aragonite $CaCO_3$ [1–4], and thus called calcareous deposit. The increase of pH at the steel/seawater interface is due to the increase of the cathodic reaction rate, a direct consequence of the cathodic polarization. In most cases, the main reaction involved is the reduction of dissolved O_2:

$$O_2 + 2H_2O + 4e^- \rightarrow 4OH^- \quad (1)$$

The production of OH^- ions increases the pH, which modifies the inorganic carbonic equilibrium at the steel/seawater interface:

$$OH^- + HCO_3^- \rightarrow H_2O + CO_3^{2-} \quad (2)$$

This process finally leads to the precipitation of $CaCO_3$ on the steel surface:

$$Ca^{2+} + CO_3^{2-} \rightarrow CaCO_{3(s)} \quad (3)$$

The growth of the calcareous deposit promotes a physical barrier against O_2 diffusion so that the current density required for CP decreases with time. This phenomenon could strongly influence the ohmic drop inside a channel of small dimension, such as the one considered in the present study, and thus modify drastically the potential of the metal deep inside the channel.

To our best knowledge, only one study devoted to a similar topic was reported [5]. It aimed to compare experimental results with a computational analysis based on boundary element modelling. Our purpose was to provide more detailed experimental results. In particular, the aim was to monitor over time the potential of the various steel coupons present inside the channel and to assess the efficiency of CP for each coupon. A 3.5-month experiment was then carried out. At the end of the experiment, a surface analysis by X-ray diffraction was achieved to characterize the calcareous deposit formed on the steel coupons. Finally, to estimate CP efficiency, polarization curves were acquired for various coupons along the channel. As performed in previous studies dealing with cathodic protection of steel in soil [6–9], the residual corrosion rate of the metal at the protection potential E_{CP} was estimated by extrapolation of the anodic Tafel straight line down to E_{CP}.

2. Materials and Method

2.1. Description of the Experimental Device Used for the Study

The experimental device was designed so that seawater flows in a channel 50 cm long, 5 mm deep and 5 cm wide, except in a 12 cm long central region, where its width was reduced to 1.5 cm. The channel was machined in one of the two Plexiglas plates (2 cm thick) that constituted the body of the device, as illustrated in Figure 1.

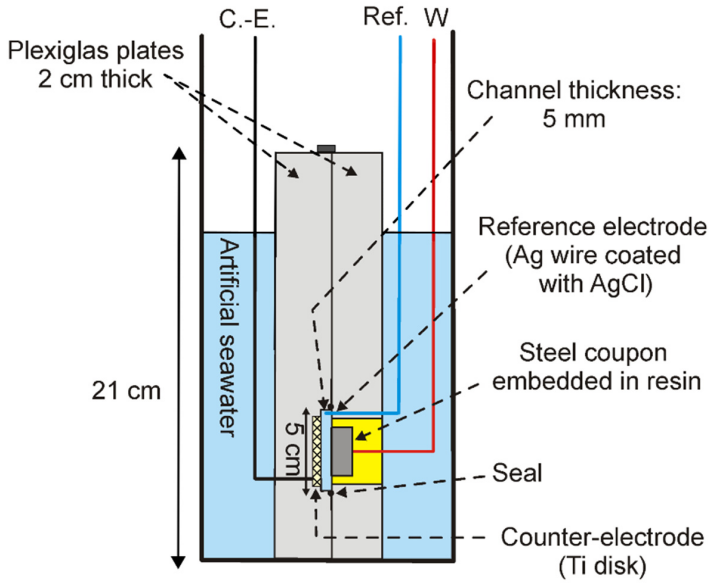

Figure 1. Schematic view (front) of the experimental device showing the respective positions of the steel coupon (grey rectangle) embedded in resin (in yellow), the Ag/AgCl microelectrode (in blue) and the Ti disk used as counter-electrode (hatched rectangle). C.-E., Ref. and W denote the three connections to the potentiostat.

In one of the Plexiglas plates, 12 large holes were drilled to insert 12 carbon steel coupons embedded in a resin matrix, as displayed in Figure 2. These coupons are denoted C1 to C12, with C1 being the coupon at the entry of the channel, where seawater comes in. A copper wire was welded on the rear side of each coupon so that the coupon could be connected to potentiostat #1 that ensured CP. Two kinds of coupons were used, with eight 3-cm diameter coupons in the 5-cm wide parts of the channel and four 1.5-cm diameter coupons in the 1.5-cm wide central part of the channel (Figure 2). The device was set in a tank (120 cm long × 25 cm deep × 15 cm wide) composed of three sections, separated by Plexiglas walls ensuring the sealing of each section. The first section, which can be called the "input section", was filled with artificial seawater. A counter-electrode (titanium grid), and an Ag/AgCl-seawater reference electrode (E_{ref} = +0.250 V vs. SHE) were set in this section and connected to potentiostat #1 used for CP. Five additional large (7 cm × 7 cm × 0.8 cm) steel plates were also immersed in the "input section" to constitute the outer part of the "simulated steel structure". They were connected to potentiostat #1 like the coupons inside the channel and thus protected similarly. The cathodic protection was applied at a constant potential of −1060 mV vs. Ag/AgCl-seawater (i.e., −1050 mV vs. SCE) with respect to the reference electrode set in the "input section". This potential value is the lowest value that could reach a steel structure connected to an Al-Zn-In galvanic anode.

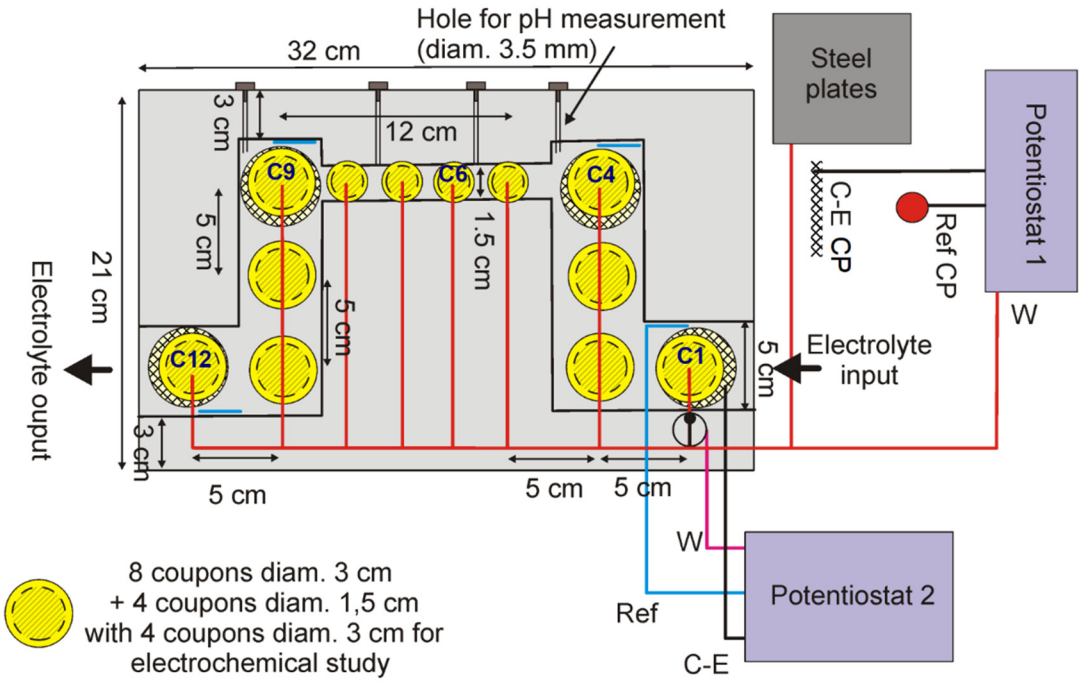

Figure 2. Schematic view (side) of the experimental device, showing the electrical connections and the positions of the four Ag/AgCl microelectrodes (blue lines) set in the channel close to coupons C1, C4, C9 and C12.

The central section of the tank, where the Plexiglas device was set, was not filled with seawater, to facilitate the visual observation of the coupons inside the channel. The third section, i.e., the "output section", was filled with artificial seawater like the "input section". An aquarium pump was placed at the bottom of this section and connected to the channel of the device via a 3-mm diameter plastic tube. The pump ensured a continuous seawater flow inside the channel at a rate, controlled weekly during the 3.5-month experiment, measured between 16 L h^{-1} and 28 L h^{-1}. The corresponding flow velocity was then between 1.8 cm s^{-1} and 3.1 cm s^{-1} in the main part of the channel and between 5.9 cm s^{-1} and 10.4 cm s^{-1} in the smaller central section.

The pumped seawater was transported up into a second tank, initially filled with a large volume of seawater. The seawater level of this thank remained constant as the

excess seawater overflowed into the "input section" of the first tank. The overall volume of seawater was equal to 20 L. Half of this volume, i.e., 10 L, was renewed after 2 weeks, after 1 month and after 2 months of experiment. A picture of the entire experimental system is shown in Figure 3.

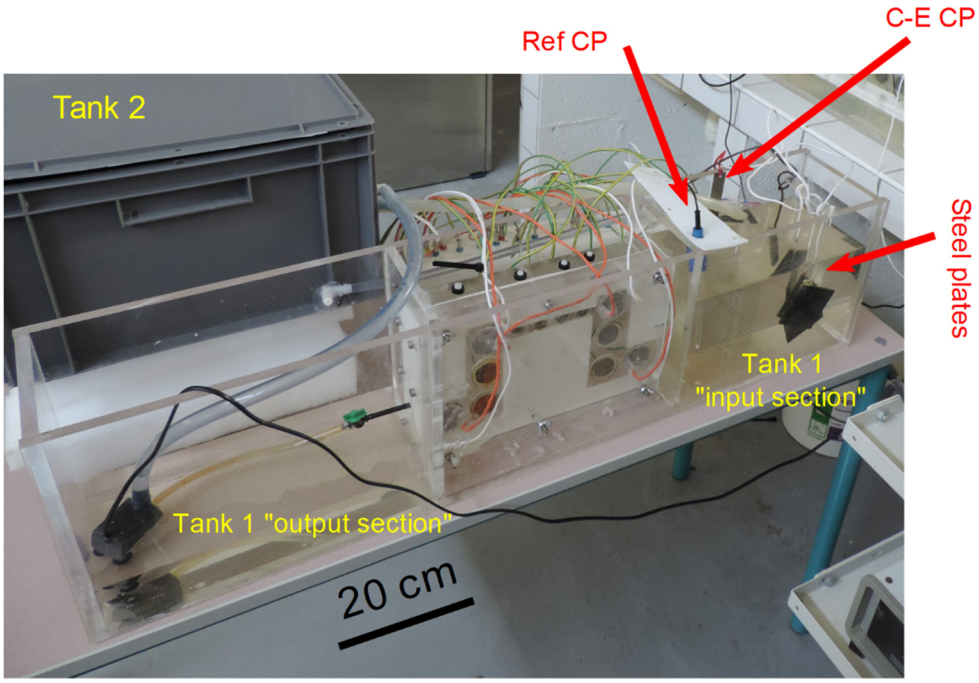

Figure 3. Image of the "real" experimental system while operating.

Four of the coupons, namely C1, C4, C9 and C12, could be disconnected individually and studied separately using a second potentiostat. Close to each coupon, an Ag wire covered with an AgCl layer was set inside the channel to be used as a local Ag/AgCl-seawater reference electrode specific to each coupon. Opposite to each of these four steel coupons, a Ti disk was inserted in the Plexiglas plate where the channel was machined to be used as a local counter-electrode (Figure 1).

Finally, four small holes (3.5-mm diameter) were drilled on top of the device so that a micro pH electrode could be inserted inside the channel for local pH measurements close to coupons C4, C6, C7 and C9 (Figure 2). The holes were closed with small rubber lids except when pH measurements were carried out.

The artificial seawater used here was based on the ATSM D1141 standard [10]. Its composition was NaCl (0.42 mol L^{-1}), $MgCl_2 \cdot 6H_2O$ (0.055 mol L^{-1}), $Na_2SO_4 \cdot 10H_2O$ (0.029 mol L^{-1}), $CaCl_2 \cdot 2H_2O$ (0.011 mol L^{-1}), KCl (0.009 mol L^{-1}) and $NaHCO_3$ (0.003 mol L^{-1}). Its pH was adjusted at 8.1 $\pm$ 0.1 by addition of small amounts of a 0.1 mol L^{-1} NaOH solution. Its conductivity was measured at 55.4 $\pm$ 0.2 mS/cm, i.e., a typical value for seawater.

S235-JR carbon steel rods (3-cm and 1.5-cm diameter) were used to prepare the coupons. The steel composition (wt %) was 98.2% Fe, 0.122% C, 0.206% Si, 0.641% Mn, 0.016% P, 0.031% S, 0.118% Cr, 0.02% Mo, 0.105% Ni and 0.451% Cu. The steel surface was abraded with silicon carbide (grade 180, particle size 80 µm), rinsed with deionized water, and carefully dried just before the coupons were set in the experimental device. The large steel plates immersed in the "input section" of tank #1 (Figures 2 and 3) were made of the same steel and their surfaces were prepared the same way.

The experiment was performed twice for 3.5 months, after an initial shorter experiment of 21 days, at room temperature (22 $\pm$ 2 °C) in each case. These experiments gave similar results but the article is focused on the last of the three experiments because, in particular, additional information about coupon C6 was only acquired in this case (see Section 2.2).

2.2. Electrochemical Measurements

When the ohmic drop is important, the "real" potential of the metal differs significantly from the applied potential E_{app}. This potential is the potential corrected from ohmic drop, $E_{IR\ free}$, expressed as:

$$E_{IR\ free} = E_{app} - RI \quad (4)$$

In Equation (4), R is the resistance of the electrolyte that separates the reference electrode from the working electrode (steel coupon), and I the current required for CP. For a cathodic current, the value of I is considered negative, which implies that $E_{IR\ free} > E_{app}$.

In our experimental conditions, E_{app} is equal to −1060 mV vs. Ag/AgCl-seawater. It corresponds to the electric voltage between each coupon under CP and the reference electrode used for CP, immersed in the "input section" of tank #1.

The potential $E_{IR\ free}$ of coupons C1, C4, C9 and C12 could be measured using potentiostat #2 via the determination of the electric voltage between the coupon and the paired Ag/AgCl-seawater microelectrode set nearby inside the channel. These measurements were performed daily during the first 20 days, weekly until day 81 and one last time at the end of the experiment (day 109). In this last day, an additional measurement was performed for coupon C6 using a hole designed for pH measurement to set an Ag/AgCl-seawater microelectrode close to the coupon.

On the last day of experiment, polarization curves were acquired for coupons C1, C4, C9 and C12 using the associated counter-electrode and Ag/AgCl-seawater microelectrode. It was also achieved for C6, using an Ag/AgCl-seawater microelectrode as explained above and the closest counter-electrode, i.e., the one facing coupon C4. The curves were obtained from $E_{IR\ free}(1) = -1.10$ V vs. Ag/AgCl-seawater to $E_{IR\ free}(2) = -0.60$ V vs. Ag/AgCl-seawater, at a scan rate $dE/dt = 0.1$ mV/s. Potentiostats #1 and #2 were both VSP potentiostats (BioLogic, Seyssinet-Pariset, France). The polarization curves were measured with the water still flowing in the channel and CP was not interrupted before the polarization curve was acquired. The lowest potential (−1.1 V vs. Ag/AgCl-seawater) was chosen to be only slightly smaller than the applied potential E_{app}, so that water reduction remained negligible. The highest potential (−0.6 V vs. Ag/AgCl-seawater) was chosen so that in any case a sufficiently large anodic region could be investigated.

All pH measurements were performed with a Mettler-Toledo micro pH electrode (Mfr # 51343160) and a SevenExcellence pH meter S400 (Mettler-Toledo SAS, Viroflay, France). They were carried out at day 28 while the seawater flow inside the channel had, exceptionally, stopped, and every two weeks with seawater flowing normally inside the channel.

2.3. X-ray Diffraction Analysis

After the experiment, the surface of the coupons was analysed by X-ray diffraction (XRD). The coupons were directly set in the sample holder and the analysis was carried out with a classical powder diffractometer (Brucker AXS® D8-Advance), using Cu-Kα wavelength (λ = 0.15406 nm) in Bragg-Brentano geometry. The acquisition was performed at 40 kV and 40 mA, from $2\theta = 10^\circ$ to $2\theta = 70^\circ$, with an angular interval of 0.04° and a counting time of 3 s per angular position.

The various phases were identified using the ICDD-JCPDS-PDF-2 database (ICDD, Newtown Square, PA, USA) via the files 01-075-2230 (aragonite = $CaCO_3$), 00-005-0628 (halite = NaCl), 01-044-1415 (lepidocrocite = γ-FeOOH) and 03-065-4899 (α-Fe).

3. Results

3.1. pH Measurements

Table 1 lists the pH values measured inside the channel at the vicinity of coupons C4, C7 and C9 and outside the channel, in the "input section" of tank #1. The value measured outside the channel was in any case between 7.8 and 8.0. At days 33 and 53, the measurements were performed with seawater flowing normally inside the channel and the

values obtained for coupons C4 and C7 were identical (or did not differ significantly) to those measured outside the channel. In contrast, the pH measured near coupon C9 was always slightly higher.

Table 1. Local pH measurements. The accuracy was estimated at ±0.1 pH via three successive measurements.

Measurement Time	pH of Seawater [1]	pH Close to C4	pH Close to C7	pH Close to C9
Day 28 (flow stopped)	7.9	8.7	9.2	9.5
Day 33	7.8	7.7	7.8	8.0
Day 53	8.0	8.0	8.0	8.5

[1] pH measured outside the channel, in the "input section" of tank #1 (see Figure 2).

On day 28, the seawater flow was accidentally stopped. It was actually observed that the 3-mm diameter tube connecting the channel to the aquarium pump (Figure 3) was clogged with rust particles coming from the insufficiently protected coupons. The measured pH values revealed that the pH was increasing all along the channel, from 8.7 close to C4 to 9.5 close to C9. This increase of pH is the consequence of CP, which increases the cathodic reaction rate and so the production of OH^- ions, as expressed by reaction (1). When the seawater flow was stopped, OH^- ions could be only transported by migration and diffusion. The observed increase of pH shows that the production of OH^- ions was sufficiently fast so that the local OH^- ions concentration could increase. Conversely, when seawater flowed inside the channel, the produced OH^- ions were also carried away by advection and could not accumulate at the vicinity of the coupons surface.

The results obtained near coupon C9 are, however, slightly different as the pH is also higher when seawater flows inside the channel. A detailed view of the experimental design is shown in Figure 4. It reveals that pH was actually measured in a corner of the channel far from the electrolyte pathway. The effects of advection in this confined region of the channel are thus insufficient to avoid the accumulation of OH^- ions.

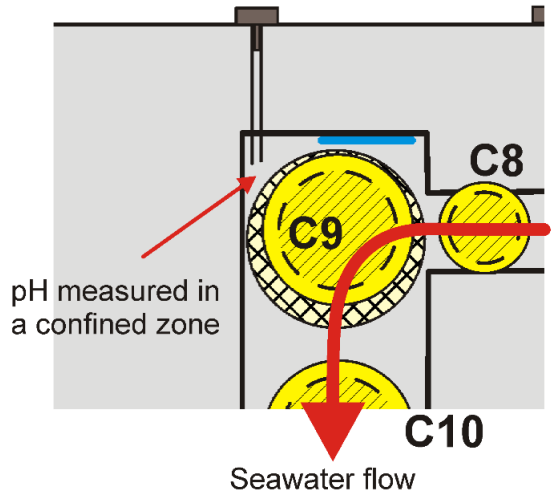

Figure 4. Schematic representation of the channel around coupon C9. The blue line corresponds to the Ag/AgCl microelectrode. The large bended red arrow displays (schematically) the water flow.

The pH was monitored all along the experiment (approximately every two weeks). For each coupon, it fluctuated around the values given in Table 1 for days 33 and 53, i.e., did not change significantly over time.

3.2. Potential Measurements

The potential corrected from ohmic drop, $E_{IR\ free}$, was measured as described in Section 2.2. for coupons C1, C4, C9 and C12. The evolution over time of these potentials is displayed in Figure 5.

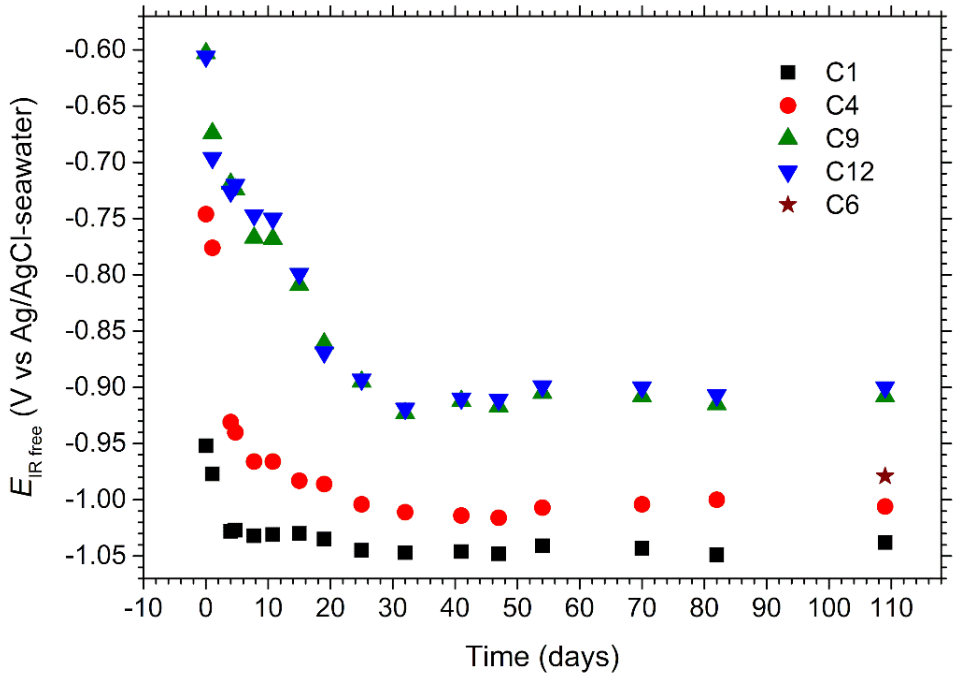

Figure 5. Evolution over time of the potential, measured with respect to the paired Ag/AgCl microelectrode, of coupons C1, C4, C9 and C12. A measurement was also performed at the end of the experiment for coupon C6 (see Section 2.2).

First, it can be seen that $E_{IR\ free}$ increases inside the channel from C1 to C12, whatever the considered time. The additional value measured for C6 at day 109 falls also between those obtained for C4 and C9, which validates the methodology used to obtain data for C6. This variation is due to the ohmic drop, which increases inside the channel as the distance from the reference electrode used to control the applied potential E_{app} increases.

Secondly, it is observed that:

$$\{E_{IR\ free}(C9) - E_{IR\ free}(C4)\} > \{E_{IR\ free}(C4) - E_{IR\ free}(C1)\} > \{E_{IR\ free}(C12) - E_{IR\ free}(C9)\}$$

This shows that the ohmic drop is the highest between C9 and C4. These two coupons are separated by the central region of the channel where the cross-sectional area is the smallest. Consequently, the electrical resistance of the electrolyte in this part of the channel is the highest. It must be recalled that the resistance R of a given volume of an electrolyte with resistivity ρ is given by:

$$R = \rho L/A \quad (5)$$

In this equation, L is the length of the electrolyte volume and A its cross-sectional area, perpendicular to the current flow (assumed uniform). For similar L and ρ, R is then inversely proportional to A. In the main part of the channel, $A = 2.5\ cm^2$, while in the central part, $A = 0.75\ cm^2$. The ratio between the two cross-sectional areas is then 3.3. At day 41, the potentials are −1.046, −1.014 and −0.912 V vs. Ag/AgCl-seawater for coupons C1, C4, and C9, respectively. This leads to $\{E_{IR\ free}(C9) - E_{IR\ free}(C4)\} = 102$ mV and $\{E_{IR\ free}(C4) - E_{IR\ free}(C1)\} = 32$ mV, thus a ratio of 3.2 between both potential differences. Note that the distance between C4 and C9 is larger than that separating C1 from C4, and that the cross section area is larger in the bends, so that the theoretical ratio between both potential differences would be actually slightly higher than 3.7.

Conversely, the cross-sectional area (and the distance L) is the same between C12–C9 and C4–C1. The associated resistance is then the same. The ohmic drop is RI and depends on the current. The counter-electrode for CP is immersed in the "input section" of tank #1 so that the current, which flows between each coupon towards the counter-electrode, flows inside the channel. Consequently, the current that flows in the C12–C9 section corresponds

to the sum of the currents required for the CP of coupons C12, C11 and C10. In contrast, the current that flows in the C4–C1 section is the sum of all currents (except that of C1). This explains why the ohmic drop is higher between C4 and C1 than between C12 and C9.

Note that the current that flows in the C9-C4 section is then smaller than the current that flows in the C4-C1 section. This explains why the measured ratio between the corresponding potential differences (i.e., 3.2) is smaller than the theoretical ratio only based on the variation of the resistance R inside the channel (~3.7).

Thirdly, it is observed that the values of the potentials were initially high and decreased with time during the first 32 days. At the beginning, the values ranged from −0.95 V vs. Ag/AgCl-seawater for C1 to −0.6 V vs. Ag/AgCl-seawater for C9 and C12. This implies that C1 was correctly protected as soon as CP was applied while the protection was insufficient for C9 and C12. This could be visually appreciated as illustrated in Figure 6. The picture was taken five days after the beginning of the experiment. Coupons C11 and C2 clearly illustrate the effects of the increase of $E_{IR\ free}$ inside the channel. C11 is obviously entirely covered by a rust layer, i.e., is not correctly protected, while C2 is covered by a whitish layer, i.e., the calcareous deposit, which demonstrates that this coupon is indeed protected against corrosion.

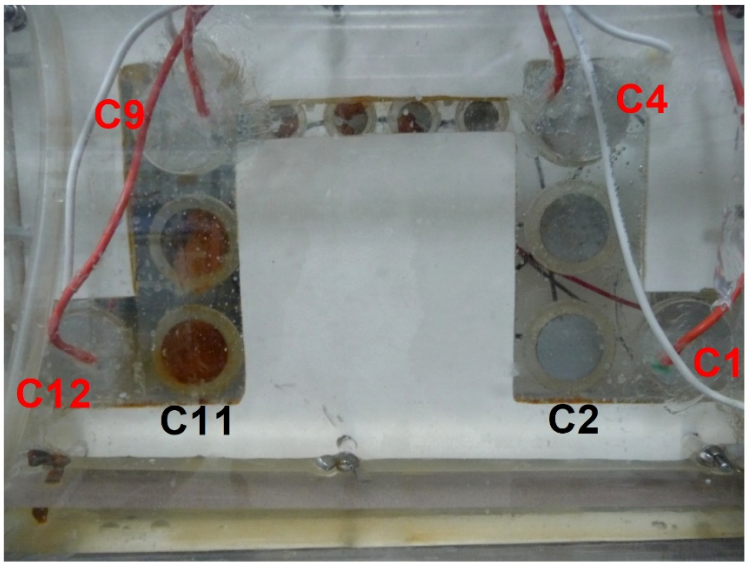

Figure 6. Image of the channel showing the surface of the steel coupons after 5 days of experiment. Coupons C1 (right of the image), C4, C9 and C12 are hidden by the corresponding counter-electrode set in the opposite side of the channel.

The potential of each coupon decreased with time during the first 32 days and stabilized afterwards. At the end of the experiment, all the $E_{IR\ free}$ values were below −0.85 V vs. Ag/AgCl-seawater, i.e., all the coupons could be considered as correctly protected according to CP standards, e.g., [11]. This decrease in potential is due to the decrease in the ohmic drop, which is necessarily due to a decrease in the current required for CP because the other parameter, i.e., the resistance of the electrolyte circuit, does not vary significantly (if at all). This decrease with time in the current required for CP is a well-known effect of calcareous deposition [1–4]. The mineral layer hinders the diffusion of O_2, decreases the active area of the metal, and thus slows down the cathodic reaction rate.

As shown in Figure 5, the potential of C1 decreased rapidly from −0.95 to −1.03 V vs. Ag/AgCl-seawater, and a calcareous deposit could form in a few days on its surface [3,4]. As shown in Figure 6, the whole surface of C2 was covered with such a mineral layer after 5 days. The decrease in the current flowing from C3, C2 and C1 consequently led to a decrease in the ohmic drop for C4 and its potential dropped from −0.75 to −0.97 V vs. Ag/AgCl-seawater after ten days. C4 was then itself progressively covered with a

calcareous deposit. The current required for CP decreased in turn for C4, then C5, C6 and so on, so that the potential of all coupons finally decreased down to an acceptable value.

To illustrate the reproducibility of the results, the potentials measured at day 18 during the three experiments (21-day experiment and two 3.5-month experiments) are given in Table 2. It can be seen that at that time, the values measured for C12 vary significantly from one experiment to the other. Coupon C12 is the farthest from the entry of the channel and its behavior depends on that of each of the other coupons. However, the values finally measured for C12 at the end of the two 3.5-month experiments were similar (about −0.9 V vs. Ag/AgCl-seawater).

Table 2. Potential values (V vs. Ag/AgCl-seawater) measured at day 18 for each of the 3 experiments.

C1	C4	C9	C12
−1.033	−0.949	not measured	−0.760
−1.015	−0.976	−0.854	−0.836
−1.034	−0.985	−0.861	−0.869

3.3. Voltammetry

The polarization curves obtained for coupons C1, C4, C6 and C9 are displayed in Figure 7. The curve obtained for C12, very similar to that of C9, was omitted for clarity.

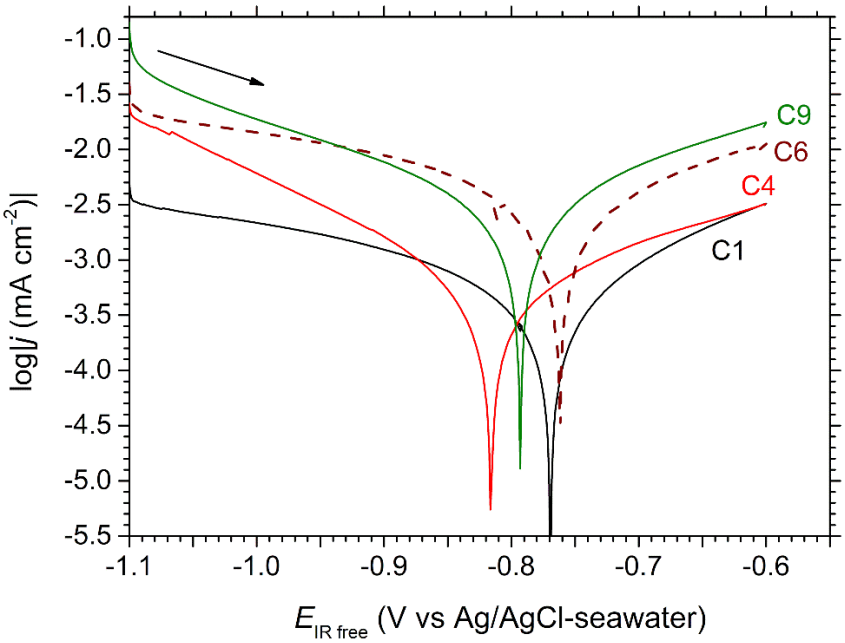

Figure 7. Polarization curves ($\log|j|$ vs. E) acquired at the end of the experiment for coupons C1 (black line), C4 (red line), C6 (brown dotted line) and C9 (green line).

First, it is observed that the corrosion potential varies between −0.82 V vs. Ag/AgCl-seawater and −0.76 V vs. Ag/AgCl-seawater, without any apparent link with the position of the coupons inside the channel. In contrast, both anodic and cathodic parts of the curves are shifted to higher current densities from C1 to C9. This evolution can be attributed to the calcareous deposit, which may be more protective for the coupons that were polarized at a lower potential during a longer time. Numerous studies devoted to calcareous deposition on steel in seawater demonstrated that a decrease in potential, in the range between −0.85 to −1.05 V vs. Ag/AgCl-seawater, led to denser and thicker layers [3,4,12]. A longer polarization time, at a given potential, also increases the thickness and decreases the porosity of the calcareous layer [3,4,13].

The anodic part of the $\log|j|$ vs. $E_{IR\ free}$ curve proved linear in any case, with similar anodic Tafel slopes, for C4, C6 and C9, (i.e., 281, 287 and 272 mV/decade) and a significantly different slope for C1 (220 mV/decade). As for the cathodic part, two behaviors can be observed. In the case of C1 and C6, the polarization curve bends progressively, from E_{cor} to more cathodic potentials, so that the slope of the curve becomes very small below −0.9 V vs. Ag/AgCl-seawater. This shows that the kinetic of the cathodic reaction, i.e., mainly O_2 reduction, is strongly influenced by mass transport. Thus, the polarization curve tends towards a diffusion plateau at the lowest potentials. In the case of C4 and C9, the influence of mass transport is less important, and the slope of the polarization curve remains high at the lowest potentials. This difference is thoroughly discussed in Section 4.

The cathodic reaction being partially controlled by diffusion, the polarization curves did not obey Tafel law in the cathodic domain. Consequently, only the anodic part of the curve was considered for an interpretation of the voltammetry results based on the Tafel method. The anodic Tafel lines were then drawn and extrapolated down to E_{CP}, i.e., the final potential reached by the coupon at the end of the CP experiment. This extrapolation led to an estimation of the corrosion current density j_{cor}, i.e., the value $j_A(E_{cor})$ of the anodic current density at $E_{IR\ free} = E_{cor}$. Similarly, the value $j_A(E_{CP})$ of the anodic current density at the potential applied during CP gave an estimation of the residual anodic current density, i.e., the residual corrosion rate, expected low, reached under CP (see references [6–9] for more details). The obtained anodic Tafel lines, drawn for each coupon between E_{cor} and E_{CP}, are displayed in Figure 8. Using Faraday's law, the obtained j_{cor} and $j_A(E_{CP})$ values could finally be converted to corrosion rates. All the obtained values (potential, current density, and corrosion rate) are listed in Table 3.

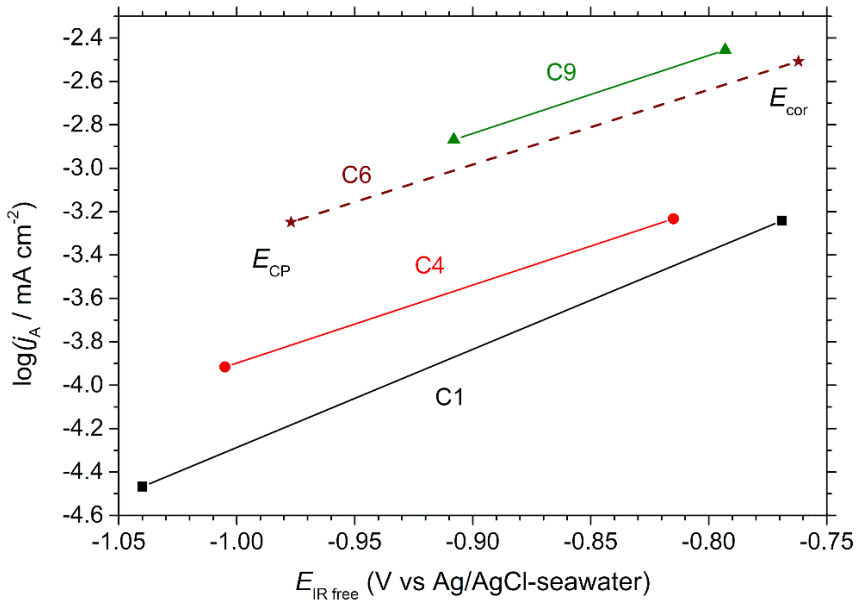

Figure 8. Anodic Tafel lines deduced graphically from the anodic branch of the polarization curves, extrapolated down to the last measured E_{CP} value, and drawn between E_{CP} and E_{cor} for coupons C1 (black line), C4 (red line), C6 (brown dotted line) and C9 (green line).

Table 3. Voltammetry measurements and data obtained via the extrapolation of the anodic Tafel line down to E_{CP}. E_{cor} is given in V vs. Ag/AgCl-seawater, j_{cor} and $j_a(E_{CP})$ in mA cm^{-2}, and the corrosion rate and residual corrosion rate in μm yr^{-1}.

Determined Parameter (Accuracy)	C1	C4	C6	C9
E_{cor} (±1 mV)	−0.769	−0.815	−0.762	−0.793
j_{cor} (±10%)	5.73×10^{-4}	5.85×10^{-4}	31.0×10^{-4}	35.0×10^{-4}
Corrosion rate (±10%)	7	7	36	41
E_{CP} (±5 mV)	−1.040	−1.005	−0.977	−0.908
$j_a(E_{CP})$ (±20%)	0.35×10^{-4}	1.21×10^{-4}	5.63×10^{-4}	13.5×10^{-4}
Residual corrosion rate at E_{CP} (±20%)	0.4	1.5	6.5	16

First, as can be seen in Figure 8 and read in Table 3, the corrosion rates of C1 and C4, almost identical, are significantly lower than those of C6 and C9, which are quite similar. This effect can be attributed to the calcareous deposit [4], which constitutes a more protective barrier against corrosion for coupons C1 and C4 polarized at lower potentials than C6 and C9 all through the experiment (see for instance Figure 5 to compare C1 and C4 with C9). The corrosion rate estimated for C1 and C4, i.e., 7 μm yr^{-1}, is actually very low, which indicates that the calcareous deposit provides an efficient protection against corrosion, at least a short time after the interruption of CP. Besides, it cannot be excluded that the increase of the interfacial pH promoted the formation of a nanometric passive or pseudo-passive layer on the steel surface.

The estimated residual corrosion rate increases from C1 to C9. As illustrated by Figure 8, this rate is not only linked to the E_{CP} values, but also to the respective positions of the anodic Tafel lines. Let us consider C6 and C9. In this case, the anodic Tafel lines are close but the E_{CP} value of C6 is significantly lower than that of C9. Consequently, CP is more efficient for C6 because the potential of this coupon is more cathodic. If we now compare C6 with C4, we can see that the E_{CP} values are not so different, but the anodic Tafel line of C4 is located at much lower current density values. In this case, CP is more efficient for C4 mainly because of the positioning of its anodic Tafel line. As explained earlier, the decrease of both anodic and cathodic current densities is due to the calcareous deposit. In other words, at the end of the experiment, CP was more efficient for C4, if compared to C6, because C4 had been previously polarized at a lower average cathodic potential, which had led to the formation of a more protective calcareous deposit (and maybe a more protective nanometric pseudo-passive layer). In the case of coupon C1, the anodic Tafel slope, different from that characteristic of coupons C4, C6 and C9 (Figure 8), is another factor that explains the very low residual corrosion rate (Table 3).

3.4. XRD Analysis

The XRD patterns obtained for coupons C7 and C9 are displayed in Figure 9.

In any case, the surface of the coupons, once extracted from the experimental device, was gently rinsed with deionized water. For the coupons covered with a fluffy layer of orange corrosion products (C11 and C12 for instance, see Figure 6), this rinsing removed most of the corrosion products. These products were analyzed separately and consisted mainly of lepidocrocite γ-FeOOH (data not shown).

Therefore, the XRD analysis reveals only the nature of the mineral layer formed on the steel surface below the orange corrosion products (if present). For all coupons, this mineral layer proved to be composed only of aragonite $CaCO_3$, as illustrated for C7, C9 and C10 in Figure 9. This is consistent with previous works dealing with calcareous deposition on steel immersed in seawater under cathodic protection [1–4].

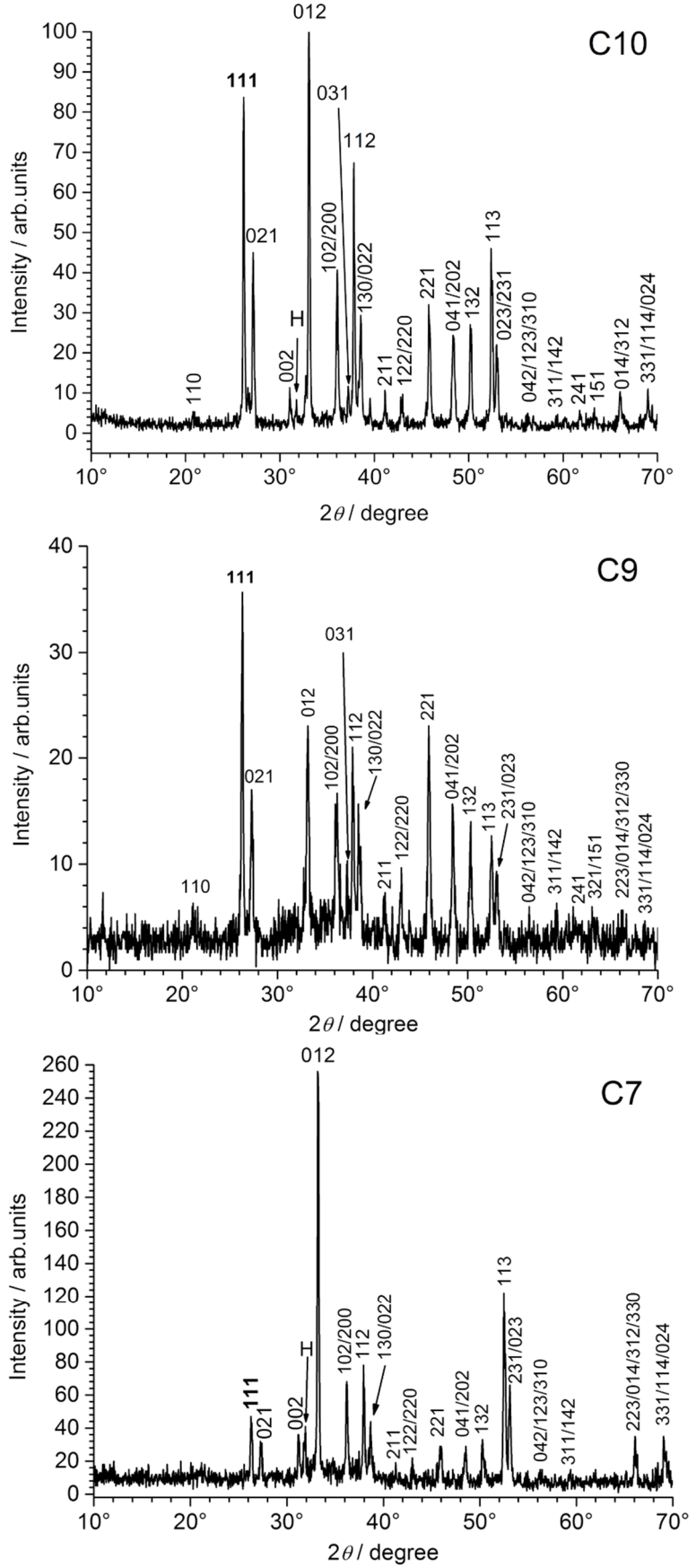

Figure 9. XRD analysis of coupons C10, C9 and C7. The diffraction lines of aragonite are denoted with the corresponding Miller index. H = main diffraction line of halite (NaCl).

When compared to the corresponding ICDD-JCPDS file, it appeared that the aragonite crystals exhibited a preferential orientation, revealed by an increased intensity of the 012 diffraction line. This phenomenon proved much more pronounced for coupons C5–C8, i.e., for the coupons set in the smaller part of the channel. The XRD pattern of coupon C7, compared to those of C9 and C10 in Figure 9, clearly illustrates this result.

4. Discussion

The experimental device was designed so that, inside a channel of small dimension filled with seawater, the ohmic drop could be important. As a result, the coupon C12 set the farthest inside the channel had an initial potential, corrected from ohmic drop, equal to $E_{\text{IR free}} = -0.61$ V vs. Ag/AgCl-seawater. The applied potential was equal to -1.06 V vs. Ag/AgCl-seawater, so that the ohmic drop was 0.45 V for C12. At the beginning, coupon C12 was not protected. Its potential however decreased during the first month and remained constant at $E_{\text{IR free}} = -0.91 \pm 0.01$ V vs. Ag/AgCl-seawater from day 32 to day 109. The decrease observed in the first month is the consequence of the formation of a calcareous deposit on the surface of the coupons located close to the channel entry, which were correctly protected as soon as CP was applied. For instance, the initial value of the potential was $E_{\text{IR free}} = -0.95$ V vs. Ag/AgCl-seawater for C1. Because of the progressive formation of the calcareous deposit, the ohmic drop decreased with time, allowing more and more coupons to be correctly protected and covered with a calcareous deposit.

At day 28, when the seawater flow inside the channel was interrupted, pH measurements demonstrated that the pH was increasing inside the channel, from C4 to C7 to C9 (Section 3.1). Because the interfacial pH is linked to the cathodic reaction rate, this result shows that the cathodic current density was increasing from C4 to C7 to C9. The already mature calcareous deposit formed on the surface of C4 implied a strongly decreased current demand. In contrast, the potential of C9 had just reached its minimal value approximately at day 28 (see Figure 5), which implies that the current demand was important. The deposit formed on C9 at higher average potential was moreover less "efficient" than the deposit formed on C4.

A steady state could, however, be reached for the whole system, approximately at day 32. This result shows that, once the deposit has formed on each coupon, and reached its "final" state (in terms of thickness and porosity), the current demand from each coupon became constant. The overall current flowing at a given position in the channel remained constant and the ohmic drop could not decrease any further. This means that the potential reached by the coupons located far inside the channel, i.e., C9–C12, could have been modelled through a theoretical computational approach only if the influence of the calcareous deposit forming on each coupon could have been modelled. Even though the modelling of calcareous deposition was already reported [13,14], this seems challenging in the present case because the effects of the calcareous deposit depend on the potential of the metal, which, in this particular problem, depends itself on the properties of the deposit formed previously on other coupons.

Moreover, coupon C6 set in the smaller part of the channel, though following the same trend observed for other studied coupons (C1, C4, C9 and C12), was characterized by two specific features. The first one relates to voltammetry: the cathodic part of the polarization curve for C6 differs from that of the polarization curves of C4 and C9. Secondly, as for the other coupons in the smaller part of the channel, XRD revealed a strong preferential orientation of the aragonite particles constituting the calcareous deposit. It can then be forwarded that the properties of the deposit formed on C6 differed from those of coupons C4 and C9. In the smaller part of the channel, the flow velocity was higher (up to 10 cm s^{-1} according to the measured flow rate), which is known to have an impact on calcareous deposition [4,12].

The efficiency of CP, assessed via voltammetry experiments, was observed to be associated not only to the cathodic level reached by a coupon at a given time, but also to the previous level of CP, that governs the protective efficiency of the calcareous deposit.

This last point is also illustrated by the low corrosion rates estimated for coupons C1 and C4 when CP was stopped (i.e., at $E = E_{cor}$). This protective ability was already observed to be important for aragonite layers [15]. It may also be partially due to the formation of a passive or pseudo-passive layer at the steel surface, favored by the increase of the interfacial pH. Such a layer would have more likely formed on the coupons polarized at the lowest potentials, and thus typically on coupon C1. This could explain the typical features of the polarization curve of coupon C1 (see Figures 7 and 8), i.e., a slightly different anodic Tafel slope and (ii) a stronger effect on O_2 diffusion in the cathodic domain (with respect to C4 and C9).

5. Conclusions

- This study demonstrated that reliable experimental data were important to understand, model and predict the behavior of steel structures involving complex geometries and seawater pathways with small dimensions. It emphasized the crucial role of calcareous deposition in the expansion of CP inside the meanders of the system.
- The formation of the deposit on the coupons located at the entry side of the channel induced a decrease of the current demand for these coupons, thus a decrease of the ohmic drop for the coupons located farther in the channel. After one month, all the coupons were correctly protected, with a potential lower or equal than −900 mV vs. Ag/AgCl-seawater in any case.
- The CP efficiency proved linked to the physical and chemical properties of the deposit. The residual corrosion rate under cathodic protection varied in the present case from <1 μm yr^{-1} to 16 μm yr^{-1}, depending not only on the potential reached by the coupon at the end of the experiment (between −900 and −1040 mV vs. Ag/AgCl-seawater), but also on the properties of the calcareous deposit formed on the steel surface.
- For the coupons polarized at the lowest potential for the longest time (e.g., C1), the beneficial influence of a nanometric passive or pseudo-passive layer at the steel surface, favored by the increase of the interfacial pH, is forwarded.

Author Contributions: Conceptualization, A.-M.G., M.J. and P.R.; Methodology, R.S., M.J. and P.R.; Validation, P.R., R.S. and M.J.; Formal Analysis, P.R., R.S. and M.J.; Investigation, P.R., R.S. and M.J.; Data Curation, P.R., R.S. and M.J.; Writing—Original Draft Preparation, P.R.; Writing—Review and Editing, A.-M.G., M.J., R.S. and P.R.; Visualization, P.R.; Supervision, A.-M.G. and P.R.; Project Administration, A.-M.G. and P.R.; Funding Acquisition, A.-M.G. All authors have read and agreed to the published version of the manuscript.

Funding: This research received no external funding.

Institutional Review Board Statement: Not applicable.

Informed Consent Statement: Not applicable.

Data Availability Statement: The data presented in this study are available on request from the corresponding author.

Acknowledgments: This study was financially supported by the IRT Jules Verne (Nantes, France) as part of the ADUSCOR research program.

Conflicts of Interest: The authors declare no conflict of interest.

References

1. Humble, R.A. Cathodic protection of steel in sea water with magnesium anodes. *Corrosion* **1948**, *4*, 358–370. [CrossRef]
2. Mantel, K.E.; Hartt, W.H.; Chen, T.Y. Substrate, Surface Finish and Flow Rate Influences Upon Calcareous Deposit Structure and Properties. In Proceedings of the Corrosion NACE Conference 1990, NACE International, Houston, TX, USA, 9–14 March 1990; p. 374.
3. Barchiche, C.; Deslouis, C.; Festy, D.; Gil, O.; Refait, P.; Touzain, S.; Tribollet, B. Characterization of Calcareous Deposits in Artificial Sea Water by Impedance Techniques. 3- Deposit of $CaCO_3$ in the presence of Mg(II). *Electrochim. Acta* **2003**, *48*, 1645–1654. [CrossRef]

4. Hoseinieh, S.M.; Shahrabi, T.; Ramezanzadeh, B.; Farrokhu Rad, M. The role of porosity and surface morphology of calcium carbonate deposits on the corrosion behavior of unprotected API 5L X52 rotating disk electrodes in artificial seawater. *J. Electrochem. Soc.* **2016**, *163*, C515–C529. [CrossRef]
5. Krupa, M.; Hogan, E.; Lemieux, E.; Seelinger, A. Cathodic Protection of Highly Complex and Shielded Components. In Proceedings of the Corrosion NACE Conference 2006, NACE International, Houston, TX, USA, 12–16 March 2006; p. 06109.
6. Barbalat, M.; Lanarde, L.; Caron, D.; Meyer, M.; Vittonato, J.; Castillon, F.; Fontaine, S.; Refait, P. Electrochemical determination of residual corrosion rates of steel under cathodic protection in soils. *Corros. Sci.* **2012**, *55*, 246–253. [CrossRef]
7. Barbalat, M.; Caron, D.; Lanarde, L.; Meyer, M.; Fontaine, S.; Castillon, F.; Vittonato, J.; Refait, P. Estimation of residual corrosion rates of steel under cathodic protection in soils via voltammetry. *Corros. Sci.* **2013**, *73*, 222–229. [CrossRef]
8. Nguyen, D.D.; Lanarde, L.; Jeannin, M.; Sabot, R.; Refait, P. Influence of soil moisture on the residual corrosion rates of buried carbon steel structures under cathodic protection. *Electrochim. Acta* **2015**, *176*, 1410–1419. [CrossRef]
9. Olubambi, P.A.; Mjwana, P.; Jeannin, M.; Refait, P. Study of overprotective-polarization of steel subjected to cathodic protection in unsaturated soil. *Materials* **2021**, *14*, 4123. [CrossRef] [PubMed]
10. *ASTM D1141-98(2021)*; Standard Practice for Preparation of Substitute Ocean Water. ASTM International: West Conshohocken, PA, USA, 2021.
11. *BS EN 12473:2014*; General Principles of Cathodic Protection in Sea Water. The British Standards Institution: London, UK, 2016.
12. Wolfson, S.L.; Hartt, W.H. An initial investigation of calcareous deposits upon cathodic steel surfaces in sea water. *Corrosion* **1981**, *37*, 70–76. [CrossRef]
13. Yan, J.-F.; Nguyen, T.V.; White, R.E.; Griffin, R.B. Mathematical modeling of the formation of calcareous deposits on cathodiccally protected steel in seawater. *J. Electrochem. Soc.* **1993**, *140*, 733–742. [CrossRef]
14. Sun, W.; Liu, G.; Wang, L.; Li, Y. A mathematical model for modeling the formation of calcareous deposits cathodically protected steel in seawater. *Elec. Acta* **2012**, *78*, 597–608. [CrossRef]
15. Möller, H. The influence of Mg^{2+} on the formation of calcareous deposits on freely corroding low carbon steel in seawater. *Corros. Sci.* **2007**, *49*, 1992–2001. [CrossRef]